Indirect Readout of the *trp*-Repressor−Operator Complex by B-DNA's Backbone Conformation Transitions†

Bernd Wellenzohn, Wolfgang Flader, Rudolf H. Winger, Andreas Hallbrucker, Erwin Mayer, and Klaus R. Liedl*

Institute of General, Inorganic and Theoretical Chemistry, University of Innsbruck, Innrain 52a, A-6020 Innsbruck, Austria

Received August 6, 2001; Revised Manuscript Received December 4, 2001

ABSTRACT: Although the *trp*-repressor−operator complex is one of the best studied transcriptional controlling systems, some questions regarding the specific recognition of the operator by the repressor remain. We performed a 2.35 ns long molecular dynamics simulation to clarify the influence of the two B-DNA backbone conformational substates B_I and B_{II} on complexation. The *trp*-repressor−operator is an ideal biological system for this study because experimental results have already figured out that the interaction between the internucleotide phosphates and the protein is essential for the formation of the high affinity complex. Our simulation supports these results, but more important it shows a strong correlation between the B_I/B_{II} phosphate substate and the number of interactions with this phosphate. In particular the $B_I \rightleftharpoons B_{II}$ transitions occur synchronous to hydrogen bond breaking or formation. To the best of our knowledge, this was observed for the first time. Thus, we conclude that the sequence specific B_I/B_{II} behavior contributes via indirect readout to sequence specific recognition. These results have implication for the design of transcription-controlling drugs in view of the recently published influence of minor groove binders on the B_I/B_{II} pattern. The simulation also agrees with crystallographically observed hydration sites. This is consistent with experimental results and indicates the correctness of the model used.

The *trp*-repressor of *Eschericia coli* is a control element in the biosynthesis of tryptophan. The binding of the repressor to the *trp*-operon, encoding the five enzymes (*trp*EDCBA, *trp*R, *alo*L, *aro*H, and *mtr*) that convert chorismate into tryptophan, is mediated by binding of corepressor. The corepressor L-tryptophan (*1*, *2*) itself binds at high concentrations ($\sim\mu$M) to the aporepressor increasing the binding affinity (*3*, *4*) of the so built repressor to the operator site, and thus prevents the transcription of these genes (negative transcriptional regulation). The first X-ray structure (Figure 1) of the *trp*-repressor−operator complex was determined by Otwinowski et al. (*5*) and shows that the *trp*-repressor binds as a dimer, and that each monomer consists of six α-helices called A, B, C, D, E, and F. The helices D and E of each monomer form a helix−turn−helix (HTH) recognition motif interacting with the major groove of the operator DNA. In the aporepressor dimer, the two HTH motifs are too close to fit into two successive binding sites in the major groove. Binding of L-tryptophan induces conformational changes that increase the distance between these HTH subunits by about 8 Å so that they fit exactly in the adjacent major grooves. The X-ray structure also suggests that the repressor dimer binds to the 18-base pair consensus operator sequence with a 1:1 stoichiometry.

Beside this so-called "traditional" or "classical" binding mode, a second different binding model (2:1 stoichiometry) was investigated (*6*) claiming that the operator sequence chosen for the crystallographic experiments of Otwinowski et al. (*5*) was not correct. Subsequent experimental studies could figure out that the operator sequence used in the original crystal studies is the preferred target for the *trp*-repressor (*4*). Additionally, the tandem *trp*-repressor−operator structure reported by Lawson and Carey (*7*) preserves on one hand the protein DNA interface of Otwinowski's X-ray structure and on the other hand both structures have nearly identical backbone conformations. For these reasons, we believe that the "traditional" binding mode of Otwinowski et al. (*5*) shown in Figure 1 is a valid model for describing the complexation.

The analysis of this protein−DNA complex (Figure 1) gives a surprising picture of the nature of the interactions. Only one direct contact (in each half site) of the amino acids with the DNA bases (G_{-9}−Arg_{69}) is observed in the X-ray structure, and NMR data (*8*) detect only few other direct hydrogen bonds to base pair functional groups. Additionally, five water mediated base amino acid side chain contacts (*9*−*11*) of each half site can be observed with both NMR and crystallographic methods. All these contacts together would not be able to explain sufficiently the high affinity and sequence specificity of the interaction. Thus, an indirect readout of the DNA was proposed to explain the sequence specificity. Indirect readout is mediated by sequence dependent conformational deformability of the DNA. The role of bending, unwinding, and other recognition tools in the indirect readout have been investigated extensively (*12*−*26*).

Smith et al. (*27*) probed the importance of the interactions of the protein with the unesterified oxygens (*28*, *29*). By using diastereomeric methylphosphonate analogues, they could show that the two unesterified oxygens of the DNA

† This work was supported by a grant of the Austrian Science Fund (Grant Number P13845-TPH).

* Corresponding author.

10.1021/bi015642t CCC: $22.00
Published on Web 02/27/2002

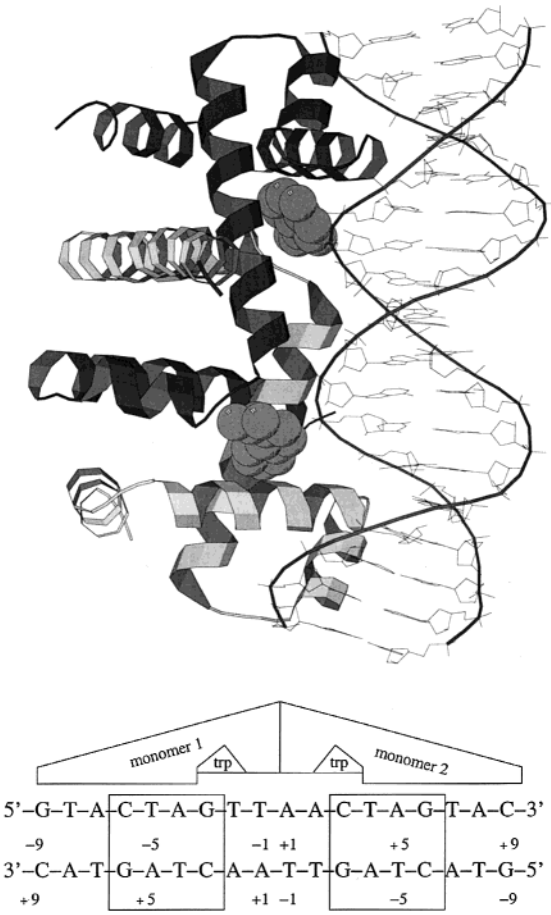

FIGURE 1: The first X-ray structure (top) of the *trp*-repressor−operator complex determined by Otwinowski et al. (*5*) shows that the repressor binds to the operator DNA as a dimer (gray and dark gray) with a 1:1 stoichiometry. The corepressor L-tryptophan (spacefill) itself acts as a wedge in each monomer. The bottom plot gives a schematic picture of the complex and indicates the two operator half tetrads (5′-CTAG-3′) necessary for repression. The numbering scheme used in the graph belongs to the 5′ → 3′ direction.

phosphates are able to contribute to binding in a different way. For example, the substitution of the phosphate linkage between $A_{+1}-P-A_{+2}$ by the S_P methylphosphonate (Figure 2 left) exhibits a slight decrease in the affinity (about 3-fold), while the R_P diastereomer exhibits a 25-fold decrease of the K_D (Figure 2, right).

Smith et al. (*27*) could attribute these different influences on complexation to specific contacts of the protein to only one of the phosphate oxygens according to the X-ray structure. The contribution of one single phosphate contact has been previously estimated and is about 1.3 kcal/mol (*30*, *31*). In addition in the *trp*-repressor−operator complex, there are 24 such contacts to unesterified phosphate oxygens, which is by far more than contacts to the bases. In view of the importance of these interactions with the phosphates, the exact DNA backbone conformational behavior is of great interest.

Different experimental (*32*−*35*) and theoretical (*36*−*38*) methods showed the existence of two B-DNA backbone conformational substates called B_I and B_{II} depicted in Figure 3. The B_I/B_{II} substates are defined by the ϵ and ζ angles of the DNA backbone or by the angle difference ($\epsilon - \zeta$). In the B_I-state, the corresponding ϵ and ζ angles are between

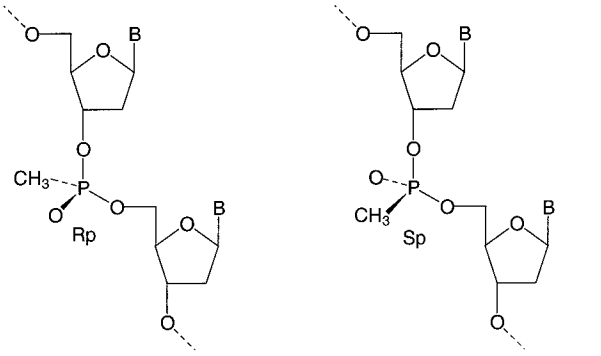

FIGURE 2: The chemical structure of the R_P (left) and S_P (right) methylphosphonates. By substituting the normal phosphates with these methylphosphonates, the *trp*-repressor is only able to make hydrogen bonds to the remaining oxygens being valuable in determining the individual influence of each unesterified DNA phosphate oxygen.

120°−210° (trans) and 235°−295°(gauche$^-$), respectively; for B_{II} the ϵ angle lies between 210° and 300° (gauche$^-$), ζ between 150°−210° (trans) (*39*−*41*). The angle difference ($\epsilon - \zeta$) is close to −90° for B_I and +90° for B_{II} phosphates (*42*).

Successful comparison of theoretical and experimental methods indicates that nowadays force fields are able to describe the B_I/B_{II} conformations in DNA properly (*33*, *36*, *38*). Investigations made by means of molecular dynamics (MD) simulation show that the B_I/B_{II} conformational substate behavior of DNA must be considered as a dynamical equilibrium (*36*, *37*, *43*) with sequence dependent properties (*36*). Detailed investigations showed that an explanation of the sequence dependence only on the dinucleotide level is insufficient.

We made a 2.35-ns MD simulation of the *trp*-repressor−operator complex to determine the possible influence of the B_I/B_{II} conformational substates on the repressor binding process. The *trp*-repressor−operator complex seems to be the ideal target for doing this because sequence specific complexation is arranged mainly by indirect readout of the DNA. The large amount of hydrogen bond contacts from the protein to the phosphate backbone provides indirect readout through these contacts. The analysis of essential protein−DNA−phosphate contacts clearly shows a correlation between the B_I/B_{II} substate and the number of hydrogen bonds to a specific phosphate. In view of the results of Smith et al. (*27*), which indicate that the removal of one hydrogen bond capability is able to decrease K_D substantially (up to 50-fold), the importance of B_I/B_{II} on the recognition process of the *trp*-repressor becomes obvious. These results together with the above-mentioned sequence dependence of B_I/B_{II} indicate that the B_I/B_{II} conformational substates could be a contributor in the indirect readout process like bending and unwinding. So, although the phosphates are chemically degenerate, they are able to transmit sequence information via the B_I/B_{II} substate conformation. Recently made MD simulation indicated that minor groove binders are able to influence the B_I/B_{II} conformational substate behavior of DNA (*37*, *43*). This elucidates the importance of the above-mentioned results for the design of transcription controlling drugs.

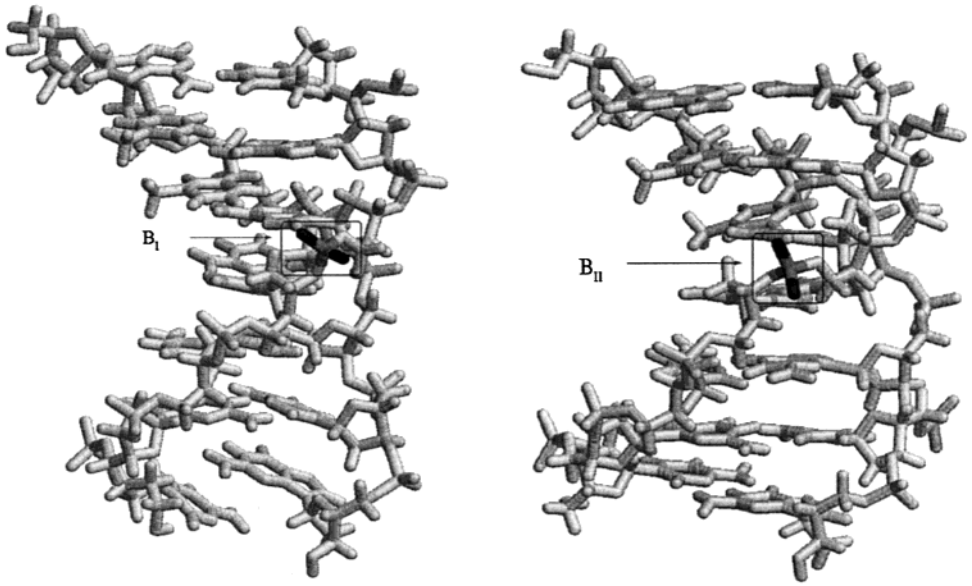

FIGURE 3: The panel on the left shows a DNA, and the phosphate indicated by the box is in the B_I conformational substate and the right panel shows the same DNA phosphate in B_{II}. In B_I, the two unesterified oxygens are looking approximately perpendicular to the helix axis, while in B_{II} these oxygens are rather parallel to the helix axis.

METHODS

MD simulations of biomacromolecules such as DNA (*44*, *45*) and DNA complexes (*37*, *43*, *46*) have proven to be a valuable tool for understanding the structural and dynamical behavior of these molecules. The inclusion of the electrostatical long range interaction via the particle mesh Ewald methods allows the accurate calculation of highly charged molecules such as DNA. Thus, stable B-form DNA trajectories could be calculated in the nanosecond time range (*47*, *48*). To take advantage of findings of previous extensive simulations (*49*, *50*), protocols employed therein were directly adapted to our needs.

The simulation of the *trp*-repressor−operator was started from the X-ray structure determined by Otwinowsky et al. (*5*) (PDB code = 1TRO). The operator octadecamer DNA has the sequence d(GTACTAGTTAACTAGTAC)$_2$, and each strand has 17 PO_4^- anions. One monomer of the *trp*-repressor dimer was simulated from residues 12 to 108 and the second monomer from 5 to 105. According to the X-ray structure, this results in a total charge of the dimer of −8. To achieve electroneutrality of the whole system, 48 positive sodium ions and 6 negative chloride ions were added using the program CION of the AMBER (*51*, *52*) package. Subsequently solvation of the whole complex with TIP3P Monte Carlo water boxes requiring a 12 Å solvent shell in all directions resulted in a system with the dimension 85.1005 × 76.4059 × 75.5096 Å^3 containing 13210 water molecules. The system has a total size of 44 153 atoms, which is a challenge due to the large computational cost. The simulation was carried out using the AMBER6 (*52*) package with the all atom force field of Cornell et al. (*53*) with the modifications by Cheatham et al. (*38*) and Wang et al. (*54*).

Minimization/Equilibration. First, 500 steps of minimization were carried out with harmonic restraints of 25 kcal mol^{-1} Å^{-2} on DNA, protein, and counterion positions. During the following five 100-step minimizations, the restraints on the counterions were relaxed faster than on DNA and the protein. Finally, 500 steps of unrestrained minimization were carried out. For equilibration, the system was heated from 50 to 300 K during 20 ps with harmonic restraints of 25 kcal mol^{-1} Å^{-2} on protein, DNA, and counterions. The harmonic restraints were reduced throughout the following 50 ps, on the counterions faster than on the oligonucleotide and ligand, by using constant-pressure and constant-temperature conditions. Finally, 10 ps unrestrained equilibration was carried out before the trajectory was generated for further 2270 ps (simulation).

General simulation parameters were kept constant during the whole simulation: 2 fs time step, SHAKE constraints of 0.00005 Å on all bonds involving hydrogen atoms, 9 Å nonbonded cutoff, and 0.00001 convergence criterion for the Ewald part of the nonbonded interactions. The temperature bath coupling was achieved by the Berendsen algorithm (*55*).

RESULTS AND DISCUSSION

The energy and the rms-deviation were used as criteria for reaching the thermodynamic equilibrium of the simulation. Figure 4 (top) shows that the energy is constant after 500 ps, indicating a stable simulation, but the rms-deviations (bottom) with respect to the starting structure increases further during the first 1.35 ns. To be sure that we obtain a reliable thermodynamical ensemble, the starting point for analysis should be at about 1.35 ns.

Nevertheless, all the following analysis plots are drawn from 80 (time after the equilibration procedure described in the methods) to 2350 ps, and the time after 1.35 ns is indicated by a box. This is done because all the features of interest to us did not show an obvious change in their behavior during the structural relaxations of the first 1.35 ns. The absolute value of the rms-deviation of 3.2 Å is very small with respect to the X-ray starting structure, taking into account the large size of the simulated system. The rms-value of the DNA alone with respect to the starting DNA is constant during the whole simulation and has a mean value of 1.47 Å.

The B_I/B_{II} conformational substate pattern as a function of time is shown in Figure 5. The line at about 1.35 ns

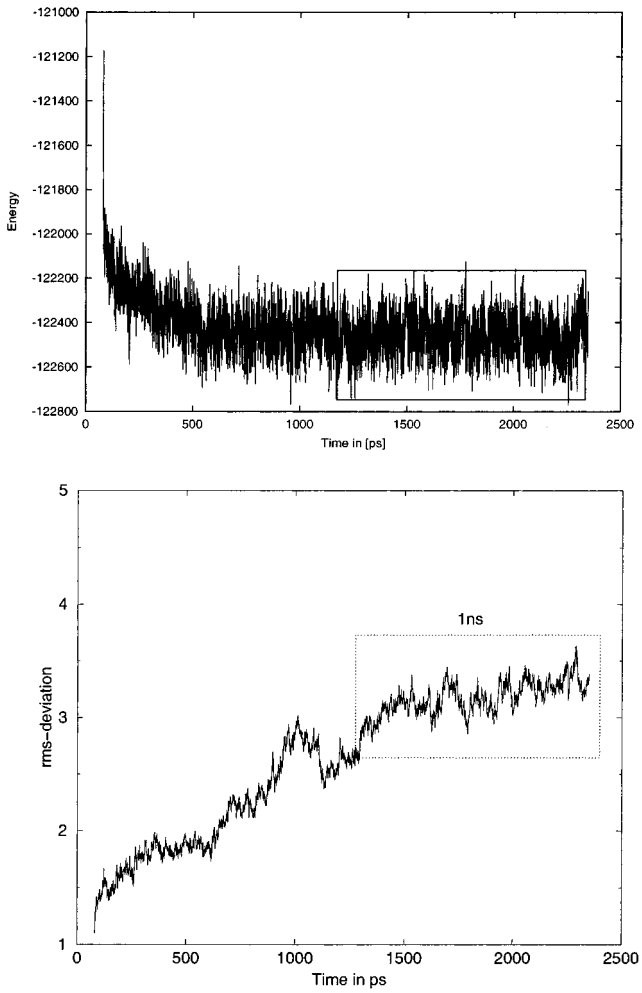

FIGURE 4: The top plot shows the total energy of the simulation against the time in (ps), and the bottom graph gives the rms-deviation (root-mean-square-deviation in Å) as function of time. While the energy is stable after about 500 ps, the rms-value changes up to about 1.35 ns. Thus, the simulation seems to be in energetic and structural equilibrium at least for the last 1 ns as indicated by the dotted box of the bottom graph.

indicates the time the system needs for reaching the structural and energetical equilibration discussed above and, as already mentioned, there is no obvious change of the substate behavior before and after reaching the equilibrium.

Figure 5 shows that the $B_I \rightleftharpoons B_{II}$ substate transitions occur in the subnanosecond time scale. In the course of the simulation, the number of phosphate groups in the B_{II} state ranges at a given time from 1 to 12. The time averaged number of base steps in B_{II} is 7.2, which is about 21%. These results are in agreement with experimental (*33*) and theoretical investigation (*38*), and they give a dynamical picture of the DNA backbone. The mechanism of these substate interconversions is described in detail elsewhere (*36*). In the crystal structure of the complex, only three phosphates are in the B_{II} state.

Due to the extraordinary importance of the protein−DNA backbone contacts in the *trp*-repressor−operator complex we analyzed the influence of the $B_I \rightleftharpoons B_{II}$ substate on the contacts. The phosphates have already shown to contribute extensively to binding (*27*). For example, the substitution of the $A_{+1}-P-A_{+2}$ linkage by the R_P methylphosphonate (see Figure 2) results in a 25-fold decrease in binding of the

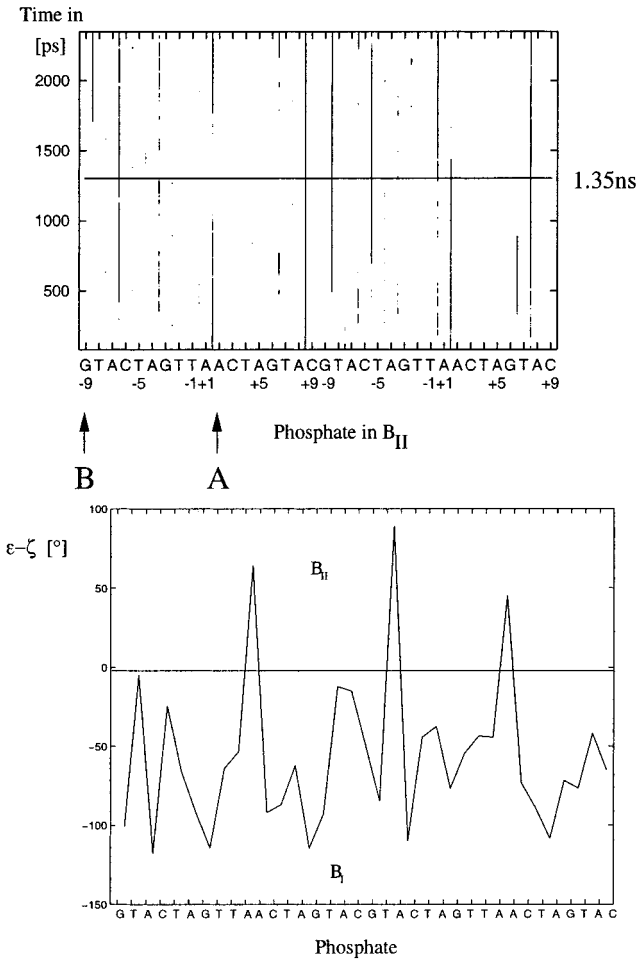

FIGURE 5: The conformational substates (B_{II}) as a function of time. The time the respective ϵ-angle is in the substate B_{II} is marked by a black line/dot. The horizontal line indicates the time at which the system reaches the structural and energetical equilibrium. The numbering scheme is according to Figure 1. A and B indicate the two phosphates that are discussed in detail in this paper. These two phosphates are chosen because they show a correlation between the B_I/B_{II} substate conformation and hydrogen bonding pattern. The bottom graph summarizes the orientation of the phosphates in the crystal structure ($+90° = B_{II}$, $-90° = B_I$).

trp-repressor, while the S_P diastereomer leads only to an about 3-fold decrease. This effect was attributed to a different interaction of Thr_{44} and Arg_{84} to the O1P and O2P unesterified phosphate oxygens. In our calculation, there is a very strong correlation (correlation coefficient greater than 0.8) between the total number of hydrogen bonds formed from Thr_{44} and Arg_{84} to the two unesterified phosphate oxygens of $A_{+1}-P-A_{+2}$ (Figure 6 top-right) and the ϵ angle as indicator for the backbone conformational substate (Figure 6 top − left). Although these results are valid for both monomers of the *trp*-repressor dimer, we discuss only the results of one dimer (indicated by arrow A in Figure 5).

First, the phosphate converts to B_{II} again at about 1.8 ns, and then the contacts are rebuilt (Figure 6). In the crystal structure, both $A_{+1}-P-A_{+2}$ phosphates are also in the B_{II} conformation, thus optimizing the hydrogen bonds (Figure 5, bottom).

Minor groove binding ligands are also able to change the B_I/B_{II} pattern of DNA (*37*), and thus we surmise that such ligands could alter binding of the *trp*-repressor even without a direct protein−ligand interaction. The AT-rich core of the

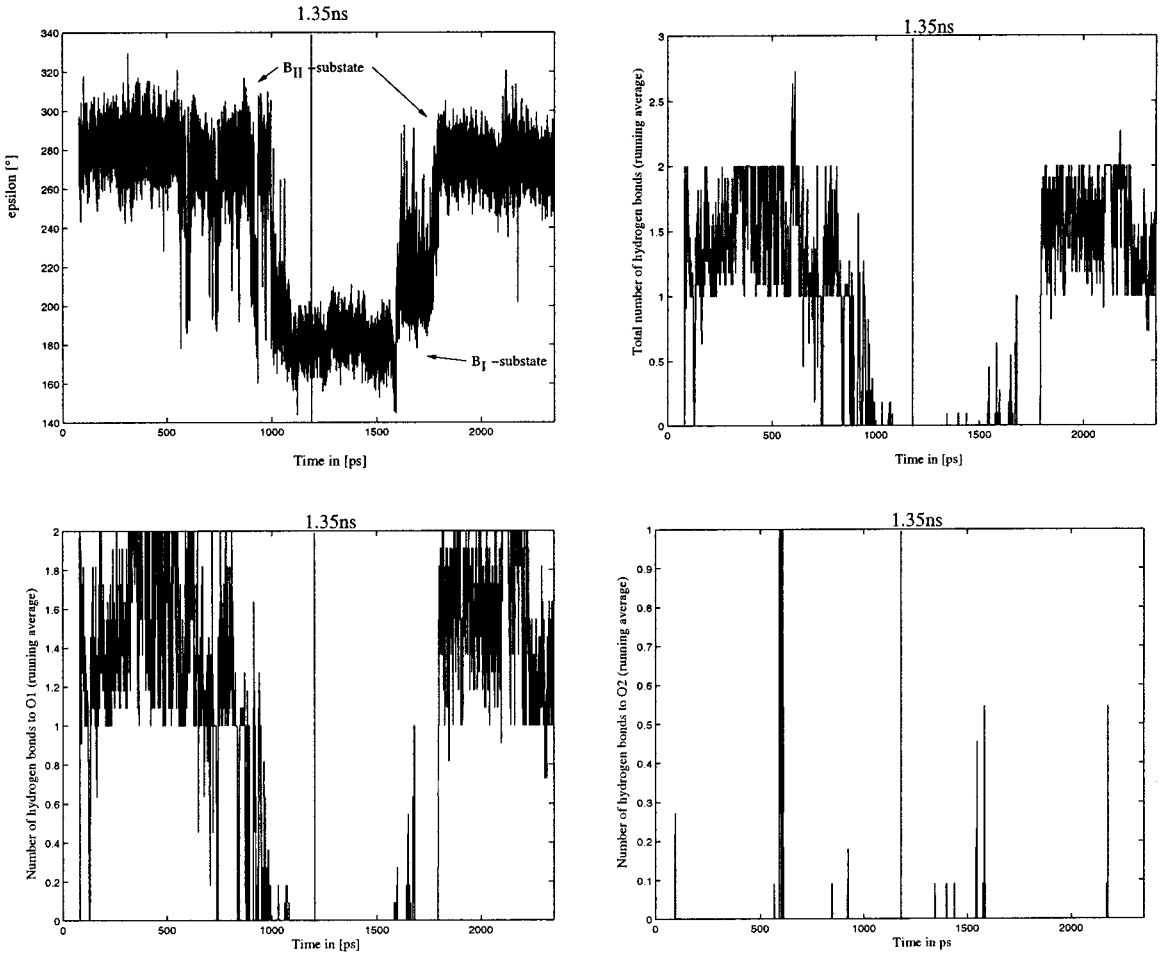

FIGURE 6: The left graph on the top shows the ϵ-torsional angle as a function of time, indicating the two backbone conformational substates B_I and B_{II}. The right graph of the top shows the number of hydrogen bonds from Thr_{44} and Arg_{84} to the phosphate oxygens of $A_{+1}-P-A_{+2}$ (the results of only one of the two steps is shown − indicated by the arrow A of Figure 5) during the simulation calculated as a running average over 10 successive snapshots (10 snapshots = 1 ps). Remember that it is not possible to have less than zero hydrogen bonds. The plots on the bottom split this information into the hydrogen bond interactions to O1 (left) and O2 (right), supporting the results of Smith et al. (*27*) that only O1 contributes extensively to binding. A contact distance shorter than 3.5 Å between a possible donor atom of the amino acids and the phosphate oxygens was interpreted as hydrogen bond.

operator should be able to bind specifically well-known ligands such as Netropsin or Hoechst33258. Recently synthesized polyamide ligands (*57*) are known to recognize specifically sequences containing the *trp*-recognition sequence 5′-GTACT-3′. This analysis also supports the explanation of Smith at al. (*27*), which makes specific contacts responsible for the different influence of the two phosphate oxygens. The oxygen O1 builds about two hydrogen bonds to the protein, while the oxygen O2 hardly forms contacts. Thus, it is easy to understand that the substitution of the R_P (=O1P) leads to a 25-fold decrease of K_D while changing S_P (=O2P) results only in a 3-fold decrease.

We further analyzed in detail the $G_{-9}-P-T_{-8}$ base step. The substitution of the unesterified phosphate oxygens of the $G_{-9}-P-T_{-8}$ step leads to a 50-fold decrease in the binding constant regardless of which methylphosphonate isomer is introduced. This experiment shows that both phosphates are contributing to the same extent to binding. In the X-ray structure (*5*), one oxygen (=O1P) interacts with Gln_{68} and Ser_{86}, while the other oxygen (=O2P) has a contact to Lys_{90}. This is consistent with the results of our simulation. Again we are discussing the results of only one of both dimers (arrow B in Figure 5) although the results are also valid for the other dimer. The number of hydrogen bonds from the amino acids to the phosphate is about the same to both phosphate oxygens O1P and O2P, and so they are degenerate in terms of contacts to the protein. At about 1.7 ns, the phosphate changes from B_I to B_{II}; this is accompanied by a total mean loss of one interacting contact (not shown). This loss is divided equally to a loss of contacts in O1P and O2P. Thus, during the simulation both phosphates are contributing to the *trp*-repressor binding to about the same extent, which is consistent with experimental studies (*27*).

In contrast to the above-mentioned interaction at the $A_{+1}-P-A_{+2}$ step, here a better contact is built with the phosphate in the more stable B_I conformation. A change of this conformation to B_{II} should reduce the binding constant. Extensive studies of the sequence dependence of B_{II}/B_I show that it is yet not able to reliably predict this conformational pattern starting from the sequence. It is not possible to rely on a prediction based on the dinucleotide steps. Even in the case of the binary B_{II}/B_I backbone arrangment, the sequence to structure correlation is extremely complicated. Thus, it is yet not possible to correlate the base substitutions with the changes in the repressor affinity (*1*) for our suggested indirect readout mechanism.

We chose the two positions $A_{+1}-P-A_{+2}$ and $G_{-9}-P-T_{-8}$ (and their counterparts of the symmetrical sequences)

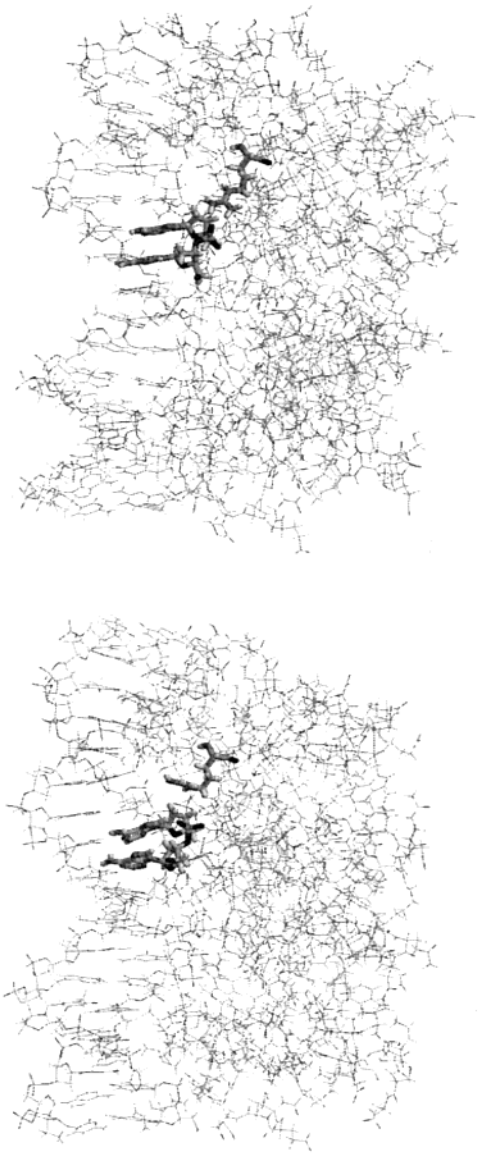

FIGURE 7: The top panel shows the $A_{+1}-P-A_{+2}$ phosphate in B_{II} and thus building hydrogen bonds with the protein. In the bottom panel, the phosphate is in the B_I conformation and has no contact to the protein. As mentioned above, only the O1 interacts with the protein, while the O2 oxygen does not contribute to complexation.

for the detailed discussions because all other phosphates either do not change their conformation during the simulation or do not show a correlation between the backbone substate conformation and hydrogen bonding pattern.

The interface between the *trp*-repressor and the operator is occupied by a large number of water molecules mediating the protein−DNA interactions. These water molecules provide a significant contribution to the free energy of binding, and their correct treatment is necessary for getting an accurate description of the complex. In our simulation, we eliminated all waters of the X-ray structure and inserted the complex in a solvation box. The analysis of the resulting simulation trajectory showed that the correct water contacts are formed independently. For example, a snapshot of the simulation (Figure 8) shows correctly the water mediated contact of Thr_{53} and Thr_{81} to the phosphate of $A_{+2}-P-C_{+3}$. This interaction is observed in the crystal structure analysis, and it implicates bridging water molecules.

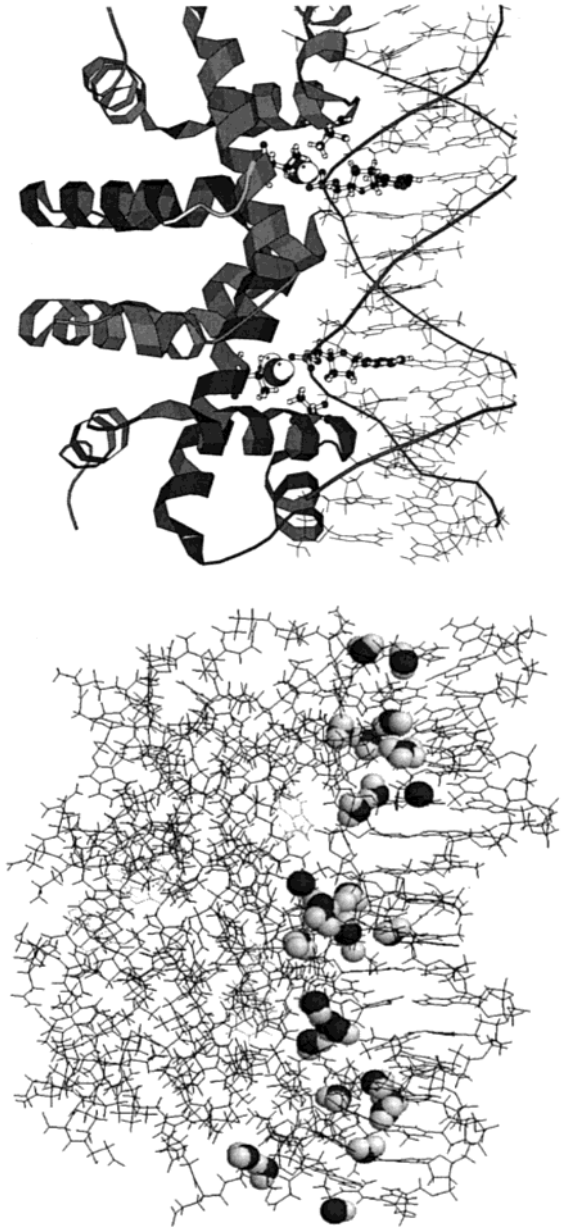

FIGURE 8: The simulation snapshot (at 1450 ps) of the top panel shows the water mediated contacts of the phosphates of $A_{+2}-P-C_{+3}$ to Thr_{53} and Thr_{81}. The waters are drawn in spacefill and the amino acid and the interacting base is indicated by balls and sticks. These water molecules remains for more than 1 ns on this position supporting this crystallographically estimated hydration site. The bottom panel shows that a variety of water molecules mediate the interaction between the *trp*-repressor and the operator.

An analysis of the residence time indicates that the water molecules of Figure 8 (top) stay for more than 1 ns at their hydration sites, which supports the above-mentioned experimental results. The bottom graph of Figure 7 indicates that the *trp*-repressor operator complexation is mediated by a variety of water molecules, again supporting well-known experimental results (*58*). In the mean of the simulation, about 50 water molecules form the interface between protein and DNA, while the respective value of the X-ray structure is about 35. A more detailed analysis of the hydration will be presented elsewhere. All together, MD simulations of protein−DNA complexes are valuable in recognizing hydration sites.

SUMMARY AND CONCLUSIONS

We performed a molecular dynamics simulation of the *trp*-repressor−operator complex to investigate the effect of the B-DNA backbone conformational substates B_I and B_{II} on complexation. Phosphate−DNA contacts contribute to a large extent to the complexation of the *trp*-repressor. The simulation shows that the number of hydrogen bond interactions directly correlates with the backbone conformational substate. The $B_I \rightleftharpoons B_{II}$ transitions occur synchronous to hydrogen bond breaking or formation. To the best of our knowledge, this was observed for the first time. Thus, we conclude that these B_I/B_{II} substates are able to play a decisive role in the sequence specific readout of the DNA. The recently published influence of minor groove binding ligands on the B_I/B_{II} pattern gives a possible scenario how such ligands could alter the binding behavior of a transcription controlling element even without a direct interaction with a protein. Additionally, our simulation is able to reproduce the experimentally observed hydration sites, which shows that MD simulations are an excellent tool for investigating these sites.

REFERENCES

1. Bass, S., Sorrells, V., and Youderian, P. (1988) *Science 242*, 240−244.
2. Carey, J. (1989) *J. Biol. Chem. 264*, 1941−1945.
3. Marmorstein, R. Q., Sprinzl, M., and Sigler, P. B. (1991) *Biochemistry 30*, 1141−1148.
4. Haran, T. E., Joachimiak, A., and Sigler, P. B. (1992) *EMBO J. 11*, 3021−3030.
5. Otwinowski, Z., Schevitz, R. W., Zhang, R.-G., Lawson, C. L., Joachimiak, A., Marmorstein, R. Q., Luisi, B. F., and Sigler, P. B. (1988) *Nature* 321−329.
6. Liu, Y.-C., and Matthews, K. S. (1993) *J. Biol. Chem. 268*, 23239−23249.
7. Lawson, L. L., and Carey, J. (1993) *Nature 366*, 178−182.
8. Zhang, H., Zhao, D., Revington, M., Lee, W., Jia, X., Arrowsmith, C., and Jardetzky, O. (1994) *J. Mol. Biol. 238*, 592−614.
9. Smith, D. A. (1994) *Modeling the Hydrogen Bond*, ACS, Washington.
10. Mazzarelli, J. M., Rajur, S. B., Iadarola, P. L., and McLaughlin, L. W. (1992) *Biochemistry 31*, 5925−5936.
11. Joachamiak, A., Haran, T. E., and Sigler, P. B. (1994) *EMBO J. 13*, 367−372.
12. Bareketh-Samish, A., Cohen, I., and Haran, T. E. (1998) *J. Mol. Biol. 277*, 1071−1080.
13. Dickerson, R. E., and Chiu, T. K. (1998) *Biopolymers (Nucleic Acid Sci.) 44*, 361−403.
14. Giese, K., Pagel, J., and Grosschedl, R. (1997) *Proc. Natl. Acad. Sci. U.S.A. 94*, 12845−12850.
15. Shi, Y., and Berg, J. M. (1996) *Biochemstry 35*, 3845−3848.
16. von Hippel, P. H. (1994) *Science 263*, 769−770.
17. Grillo, A. O., Brown, M. P., and Royer, C. A. (1999) *J. Mol. Biol. 287*, 539−554.
18. Shakked, Z., Guzikevich-Guerstein, G., Frolow, F., Rabinovich, D., Joachimiak, A., and Sigler, P. B. (1994) *Nature 368*, 469−473.
19. Steitz, T. A. (1993) *Structural Studies of Protein-Nucleic Acid Interaction*, Cambridge University Press, Cambridge, UK.
20. Lilley, D. M. J. (1995) *DNA − Protein: Structural Interactions*, Oxford University Press, Oxford, UK.
21. Travers, A. (1993) *DNA − Protein Interactions*, Chapman & Hall, London, UK.
22. Bewley, C. A., Grinenborn, A. M., and Clore, G. M. (1998) *Annu. Rev. Biophys. Biophys. Chem. 27*, 105−131.
23. Chen, Y.-Q., Gosh, S., and Gosh, G. (1998) *Nat. Struct. Biol. 5*, 67−73.
24. Ellenberger, T. (1994) *Curr. Opin. Struct. Biol. 4*, 12−21.
25. Neidle, S. (1997) *Biopolymers (Nucleic Acid Sci.) 44*, 105−121.
26. Pabo, C. O., and Sauer, R. T. (1992) *Annu. Rev. Biochem. 61*, 1053−1095.
27. Smith, S. A., and McLaughlin, L. W. (1997) *Biochemistry 36*, 6046−6058.
28. Lesser, D. R., Grajkowski, A., Kurpiewski, M. R., Koziolkiewicz, M., Stec, W. J., and Jen-Jacobson, L. (1992) *J. Biol. Chem. 267*, 24810−23818.
29. Kurpiewski, M. R., Koziolkiewicz, M., Wilk, A., Stec, W. J., and Jen-Jacobson, L. (1996) *Biochemistry 35*, 8846−8854.
30. Lohmand, T. M., deHaseth, P. L., and Record, M. T., Jr. (1980) *Biochemistry 19*, 3522−3530.
31. Jen-Jacobson, L., Lesser, D., and Kurpiewski, M. (1986) *Cell 45*, 619−629.
32. van Dam, L., and Levitt, M. H. (2000) *J. Mol. Biol. 304*, 541−561.
33. Gorenstein, D. G. (1994) *Chem. Rev. 94*, 1315−1338.
34. Grzeskowiak, K., Yanagi, K., Privé, G. G., and Dickerson, R. E. (1991) *J. Biol. Chem. 266*, 8861−8883.
35. Pichler, A., Rüdisser, S., Mitterböck, M., Huber, C. G., Winger, R. H., Liedl, K. R., Hallbrucker, A., and Mayer, E. (1999) *Biophys. J. 77*, 398−409.
36. Winger, R. H., Liedl, K. R., Rüdisser, S., Pichler, A., Hallbrucker, A., and Mayer, E. (1998) *J. Phys. Chem. B 102*, 8934−8940.
37. Wellenzohn, B., Winger, R. H., Hallbrucker, A., Mayer, E., and Liedl, K. R. (2000) *J. Am. Chem. Soc. 122*, 3927−3931.
38. Cheatham, III., T. E., Cieplak, P., and Kollman, P. A. (1999) *J. Biomol. Struct. Dyn. 16*, 845−862.
39. Schneider, B., Neidle, S., and Berman, H. M. (1997) *Biopolymers 42*, 113−124.
40. Berman, H. M. (1997) *Biopolymers 44*, 23−44.
41. Hartmann, B., and Lavery, R. (1996) *Quart. Rev. Biophys. 29*, 309−368.
42. Fratini, A. V., Kopka, M. L., Drew, H. R., and Dickerson, R. E. (1982) *J. Biol. Chem. 257*, 14686−14707.
43. Wellenzohn, B., Flader, W., Winger, R. H., Hallbrucker, A., Mayer, E., and Liedl, K. R. (2001) *J. Am. Chem. Soc. 123*, 5044−5049.
44. von Kitzing, E. (1992) *Methods Enzymol. 211*, 449−467.
45. Beveridge, D. L., and Ravishanker, G. (1994) *Curr. Opin. Struct. Biol. 4*, 246−255.
46. Perree-Fauvet, M., and Gresh, N. (1994) *J. Biomol. Struct. Dyn. 11*, 1203−1224.
47. Cieplak, P., Cheatham, III., T. E., and Kollman, P. A. (1997) *J. Am. Chem. Soc. 119*, 6722−6730.
48. Cheatham, T. E., III., and Kollman, P. A. (1996) *J. Mol. Biol. 259*, 434−444.
49. Young, M. A., Ravishanker, G., and Beveridge, D. L. (1997) *Biophys. J. 73*, 2313−2336.
50. de Souza, O. N., and Ornstein, R. L. (1997) *Biophys. J. 72*, 2395−2397.
51. Case, D. A., Pearlman, D. A., Caldwell, J. W., Cheatham, III., T., Ross, W. S., Simmerling, C. L., Darden, T. A., Merz, K. M., Stanton, R. V., Cheng, A. L., Vincent, J. J., Crowley, M., Ferguson, D. M., Radmer, R. J., Seibel, G. L., Singh, U. C., Weiner, P. K., and Kollman, P. A. (1997) *AMBER 5*, University of California, San Francisco.
52. Case, D. A., Pearlman, D. A., Caldwell, J. W., Cheatham, III., T., Ross, W. S., Simmerling, C. L., Darden, T. A., Merz, K. M., Stanton, R. V., Cheng, A. L., Vincent, J. J., Crowley, M., Tsui, V., Radmer, R. J., Duan, Y., Pitera, J., Massova, I., Seibel, G. L., Singh, U. C., Weiner, P. K., and Kollman, P. A. (1999) *AMBER 6*, University of California, San Francisco.
53. Cornell, W. D., Cieplak, P., Bayly, C. I., Gould, I. R., Merz, Jr., K. M., Ferguson, D. M., Spellmeyer, D. C., Fox, T., Caldwell, J. W., and Kollman, P. A. (1995) *J. Am. Chem. Soc. 117*, 5179−5197.
54. Wang, J., Cieplak, P., and Kollman, P. A. (2000) *J. Comput. Chem. 21*, 1049−1074.

55. Berendsen, H. J. C., Postma, J. P. M., van Gunsteren, W. F., DiNola, A., and Haak, J. R. (1984) *J. Chem. Phys. 81*, 3684−3690.
56. Berman, H. M., Olson, W. K., Beveridge, D. L., Westbrook, J., Gelbin, A., Demeny, T., Hsieh, S.-H., Srinivasan, A. R., and Schneider, B. (1992) *Biophys. J. 63*, 751−759.
57. Kielkopf, C. L., Baird, E. E., Dervan, P. B., and Rees, D. C. (1998) *Nat. Struct. Biol. 5*, 104−108.
58. Ladbury, J. E., Wright, J. W., Sturtevant, J. M., and Sigler, P. B. (1994) *J. Mol. Biol. 238*, 669−681.

BI015642T